3D zeros in electromagnetic fields

Vernon, Alex J.; Dennis, Mark R.; Rodríguez-Fortuño, Francisco J.

DOI:
10.1364/OPTICA.487333

Document Version
Publisher's PDF, also known as Version of record

Citation for published version (Harvard):
Vernon, AJ, Dennis, MR & Rodríguez-Fortuño, FJ 2023, '3D zeros in electromagnetic fields', *Optica*, vol. 10, no. 9, pp. 1231-1240. https://doi.org/10.1364/OPTICA.487333

Research Article Vol. 10, No. 9 / September 2023 / Optica 1231

3D zeros in electromagnetic fields

Alex J. Vernon,[1,3] Mark R. Dennis,[2,4] and Francisco J. Rodríguez-Fortuño[1,*]

[1]Department of Physics and London Centre for Nanotechnology, King's College London, Strand, London WC2R 2LS, UK
[2]School of Physics and Astronomy, University of Birmingham, Birmingham B15 2TT, UK
[3]alexander.vernon@kcl.ac.uk
[4]m.r.dennis@bham.ac.uk
*francisco.rodriguez_fortuno@kcl.ac.uk

Received 8 February 2023; revised 5 June 2023; accepted 18 July 2023; published 19 September 2023

We present a study of 3D electromagnetic field zeros, uncovering their remarkable characteristic features and propose a classifying framework. These are a special case of general dark spots in optical fields, which sculpt light's spatial structure into matter-moving, information-rich vortices, escape the diffraction limit for single-molecule imaging, and can trap particles for nanoscale manipulation. Conventional dark spots are 2D in two aspects: localized in a plane and having a non-zero out-of-plane field component. We focus on non-paraxial fields, where 3D dark spots can exist non-stably at fully localized points, making distinct imprints in the flux of energy and momentum, and in the light's polarization texture. With this work, we hope to enhance current dark spot applications, or inspire new ones impossible with lower-dimensional zeros.

https://doi.org/10.1364/OPTICA.487333

1. INTRODUCTION

An optical vortex is the name commonly given to a zero in a complex scalar field, such as a component of the electric **E** or magnetic **H** field. Vortices in these components occur naturally in general 3D monochromatic interference [1], where they are infinitely thin continuous strands either extending infinitely through space or coiled into knotted, un-knotted, or linked closed loops [2–5]. On a vortex strand, the phase of the complex scalar field, which has zero real and imaginary parts, is undefined. This "phase singularity" contributes a circulation, throughout all of space, to the phase of the rest of the complex scalar field. Along a closed loop containing one vortex line, the circulating phase of the field increases in a clockwise or anticlockwise sense by an integer multiple of 2π. Vortex lines in optics have direct analogs in acoustics and water waves, and as a type of topological defect, are related to vortices in (super) fluids [6] and in Bose–Einstein condensates [7], and even cosmic strings [8]. Strong research interest in optical vortices over the past 30 years, combined with the availability of instruments and the flexibility in generating [9–12] and structuring [13] vortex-carrying beams, has positioned optics to act as a sandbox for exploring topological phenomena that appear more broadly across physics.

When considering the full 3D vector characteristics of an optical field, vortex lines in individual field components such as E_x, E_y, and E_z are basis dependent and not so physically meaningful. By picturing these different scalar vortex threads permeating the vector field, we can appreciate how unlikely it is that the optical field is zero at a point (i.e., $\mathbf{E} = \mathbf{0}$, all three components simultaneously zero) in typical 3D interference (the vortex line in each of the three field components would meet at such a zero point, requiring the manipulation of three extra parameters beyond the spatial x, y, z). Despite the rarity of complete zeros in the wild, a lower-dimensional version can be readily manufactured in optical beams, and is remarkably well studied. Paraxial doughnut beams have an axial zero in the transverse field surrounded by a bright ring, and are used in modern spectroscopy techniques [14,15] because of the zero's immunity to the diffraction limit. The transverse field effectively consists of one or two scalar components with the vortex line along the beam axis, causing the real part of the local wave vector to curl around the axis and imbue the beam with intrinsic orbital angular momentum. The longitudinal field, meanwhile, is non-zero (albeit very small due to paraxiality) in the center of the beam, which, therefore, is better imagined not as an exact axial zero, but as a dim line of linear polarization (an L line) polarized parallel to the beam direction. This, and its confinement in only two dimensions, stretching along the third, is why we refer to the almost-dark center of the doughnut beam as a 2D zero. Its topological index is straightforward to define by counting how many multiples of 2π the phases of the transverse components climb through over an enclosing circuit. The intrinsic orbital angular momentum carried by doughnut beams is the key property of the spatial structure of light that can rotate matter [16,17] and store information [18–20].

Surprisingly, the fully localized, 3D optical field zero, $\mathbf{E} = \mathbf{0}$, has been left largely unexplored. This is probably due to its unstable nature—a perturbation will destroy the zero point (i.e., cause the vortices in the three components no longer to coincide). Nevertheless, such a point is theoretically possible [21] and similar

point-like singularities have been artificially synthesized [22,23], but very little is understood about how it is imprinted into the surrounding field, and there is no simple classifying topological index like the topological charge of a 2D vortex. We find that there is characteristic behavior around these field nulls—such as their organization of generic polarization singularities through them—which we investigate here.

The 3D electromagnetic field zero in its most fundamental, asymmetric, and 3D-confined form is the focus of this work. It is important to distinguish this "generic" zero as, relatively speaking, the most likely type of three-component zero (i.e., $\mathbf{E} = \mathbf{0}$) to occur naturally. It may be argued that even in non-paraxial regimes, higher-order vortex beams or azimuthally polarized beams have null longitudinal field components on their axes and a three-component zero exists there. We do not treat such high-order axial beam zeros, or those of azimuthal beams here, for two reasons. First, the zeros we study are first order, in that the first-order spatial derivatives of the field components are non-zero. Higher-order zeros fall outside of the classification we present in this work, and would require their own detailed analysis (polarization and vector singularities coupled to the high-order zero are much more complex). Second, beams are, by design and regardless of order, highly symmetric fields with degenerate polarization, momentum, and energy structures that are not normally characteristic of a typical 3D zero created in asymmetric, multiple plane wave interference. A zero in the **E**-field alone has codimension 6, requiring that the six total degrees of freedom of two real, 3D vectors (real and imaginary parts of the three components **E**) are suppressed simultaneously. This means 3D zeros exist stably in a 6D parameter space, and is why optical field zeros are not natural in random interference patterns spanning only three spatial dimensions, being hidden by instability. Instead, 3D zeros must be revealed by tuning an additional three parameters (this is discussed in [22] for a zero in two electric field components). Some of these parameters could be the polarization components of a plane wave, for example, and in fact, 3D zeros can be very easily manufactured and controlled in pure plane wave interference or near fields with a simple technique [21], and their higher dimensional confinement could provide a greater degree of precision in dark spot spectroscopy. Due to their electric field dependence, the zero in **E** is coupled to a collection of singularities, each with its own topological signature, in various physical quantities associated with the light field including the complex Poynting vector, canonical momentum, spin momentum, and spin angular momentum. Learning how energy flow and momentum circulate around a 3D vortex could inspire applications that would be otherwise unfeasible using typical lower-dimensional zeros. Alternatively, the magnetic field **H** may vanish at a point, or more extremely, both **E** and **H** might simultaneously vanish, giving a true electromagnetic null with codimension 12. Here, we report the key features of a 3D field electric or magnetic field zero, including the way that polarization singularities are forced to intersect and the flux of the complex Poynting vector and canonical and spin momenta. With these findings, for the first time, we propose a framework to classify the physically realizable varieties of 3D field zero.

2. RESULTS

To contextualize our study, we begin with some brief intuition on the special features that we might expect to find near a 3D zero. If either **E** or **H** is zero at a given point $\mathbf{r}_0$, some related quantities are zero too, including the flux of energy, canonical momentum, and spin angular momentum. Since these fluxes are vector quantities, their direction is singular at $\mathbf{r}_0$, and an imprint is made in the surrounding space where they are well defined. In three spatial dimensions, even if these fluxes are divergence-less, there is more than one possible (topologically unique) imprint that can be left by and characterize the zero in **E**. The electric field spin is particularly interesting, because its zeros (in non-paraxial fields) are codimension 2 objects—meaning they are 1D continuous lines, defining the threads of pure linear electric polarization. This continuity should require at least one zero-spin line, an L line, to pass through $\mathbf{r}_0$. A similar argument can be made for lines of pure circular electric polarization, except that C lines are defined by a complex quadratic equation, $\mathbf{E} \cdot \mathbf{E} = 0$, equivalent to a real quartic equation, $|\mathbf{E} \cdot \mathbf{E}|^2 = 0$, which has zero, two, or four real roots. It turns out, as we will show, that a given number of C lines and L lines must always intersect in a 3D electric field zero. Before reporting these and other findings in detail from a mathematical argument and analytical simulations in Section 2.3 and beyond, the next two subsections provide an overview of polarization singularities and set out our way of classifying 3D field zeros using dyadics associated with the field.

A. Overview of Polarization Singularities in Paraxial and Non-paraxial Fields

L lines and C lines are called polarization singularities and are vector versions of scalar vortex lines in wave fields, existing in light [24–26] and acoustic and water waves [27] (both acoustic and water waves have a vector nature [28,29]) where some property of the general polarization ellipse is not defined. In 3D fields, polarization singularities are often described as the underlying skeleton that embeds highly complex topologies into the field's polarization texture [30,31]. Polarization singularities have been studied in full 3D and in paraxial fields [32], where in paraxial fields (considering only the two transverse field components), polarization is circular at points and linear along lines. Propagating the paraxial field (maintaining transverse polarization) draws out the C points and L lines in the transverse plane into C lines and L surfaces in three dimensions.

A polarization ellipse has orthogonal semi-major and semi-minor axes, telling us which way the ellipse is oriented. But because a polarization circle has no semi-major or semi-minor axis, at a C point, the orientation of the circle is undefined causing neighboring polarization ellipses (almost circular) to rotate when tracked along a C-point-enclosing loop. The ellipse major axis is described throughout space with a line field, in that the axis is oriented some way in space but does not point one way or another—an ellipse looks identical to its 180 deg rotated self. This means that along the enclosing circuit, the rotating ellipses turn continuously through an integer multiple of π radians, rather than 2π, which is why C points are assigned a half-integer index. When the field is fully 3D and the polarization ellipse is free to tilt in any Cartesian direction, circular polarization still occurs along 1D threads (C lines that are no longer straight as in the paraxial case) but the surrounding polarization ellipses also twist, so that their major axes sweep out Möbius strips [33–35]. Analogs of C lines exist in polychromatic fields, shaping the rest of the field into other remarkable topological structures [36].

L lines/L surfaces in paraxial fields (ignoring longitudinal fields) separate regions of left and right handed polarization ellipses.

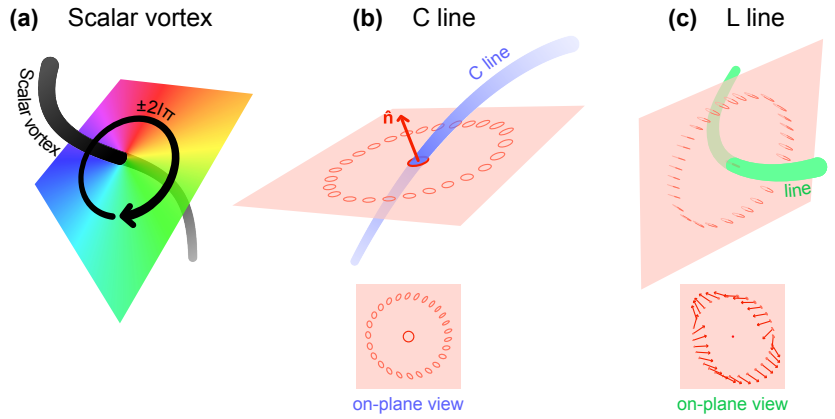

Fig. 1. Visualization of scalar and polarization singularities in a non-paraxial electromagnetic field. (a) Scalar vortices exist in complex scalar fields, such as the components of **E**, where the scalar field is zero and its phase is undefined, forming 1D threads in the interference of three or more plane waves. Around a scalar vortex line, the phase of the field increases by an integer l multiple of 2π in a clockwise or anticlockwise sense. Singular lines exist in the complex vector characteristic of **E** and **H** fields, called polarization singularities, which include C lines (lines of circular polarization) and L lines (lines of linear polarization). (b) In a circuit around a point on a C line, in the plane of the polarization circle at that point, nearby polarization ellipses rotate through an integer multiple of π radians. (c) Around an L line, the normal to nearby polarization ellipses rotate by an integer multiple of 2π radians.

In non-paraxial fields, L lines are strictly 1D lines (not surfaces) and complement C lines in shaping the surrounding polarization structure. This reduction of dimension to the L entity occurs because, to be linearly polarized, the real and imaginary parts of the field (say $\mathbf{E} = \mathbf{p} + i\mathbf{q}$) need to be (anti)parallel (not necessarily equal). If **E** is paraxial and linearly polarized, then in the transverse plane, the ratio of the x components of **p** and **q** must equal the ratio of their y components—a single condition, dissolving only one degree of freedom of one vector relative to the other. If **E** is non-paraxial, then an extra condition accounting for the ratio of the z components of **p** and **q** must be satisfied for linear polarization [23]. Between paraxial and full 3D fields, the linear polarization object's codimension increases from one to two. Its codimension is the dimension of the vector space $\mathbf{S}_{\mathrm{E}}$ (3) minus the real-space dimension of the L surface (2) or L line (1) which lies in $\mathbf{S}_{\mathrm{E}}$. The spin angular momentum of the field is zero when linearly polarized, meaning the direction of the normal to the field oscillations cannot be defined. Drawing a circuit around an L line, the spin vector rotates through 2π radians in a clockwise or anti-clockwise sense and defines the L line's topological index.

The characteristics of scalar vortices and C lines and L lines are visualized in Fig. 1.

B. Indexing Point-Like Singularities

Polarization singularities occur equally often among the general polarization ellipses in **E** and **H** fields, and need not coincide with each other. Phase singularities, C lines, and L lines are all indexed by looking at the circulation or rotation of a scalar or vector quantity around a loop enclosing the singularity of interest [37]. All three of these singularities are threads in 3D fields, but the winding number concept can be generalized to higher-dimensional singularities and calculated for point-like, 3D vector singularities via the topological degree. Instead of integrating a quantity associated with a line singularity around a 1D closed circuit, for isolated singular points in 3D, we should integrate an appropriate quantity over a closed surface enclosing the point singularity. For a vector $\mathbf{V}(\mathbf{r}_S)$ on a surface S ($\mathbf{r}_S \in S$) in 3D real space, for example, the topological degree of $\mathbf{r}_S \mapsto \mathbf{V}$ (mapping from the real space surface $\mathbf{r}_S$ to **V**) is a calculation of the integer number of times that every possible direction of **V** is realized (on a sphere) on all points $\mathbf{r}_S$ on the surface S. As with other kinds of topological singularities in physical fields, the easiest realized topological degrees (winding numbers) are ± 1. Mathematically, a $0, \pm 1$ topological degree is the integral of the determinant of the dyadic $D(\mathbf{V})$ of **V** over S divided by A, the area of S:

$$\deg(\mathbf{V}) = \frac{1}{A}\int_S \det(D(\mathbf{V}))\mathrm{d}S. \tag{1}$$

The dyadic $D(\mathbf{V})$, also called the Jacobian matrix of **V**, contains the first-order spatial derivatives of each component of **V**. The sign of the determinant of $D(\mathbf{V})$ equals the product of the signs of its eigenvalues. For 3D vectors where $D(\mathbf{V})$ is a 3×3 matrix, it is possible for drastically different behaviors of **V** to be hidden under the same topological degree. For example, if $\mathbf{V}(\mathbf{r} = 0) = \mathbf{0}$ (meaning the direction of **V** is singular at the origin) and we assume that a linear map from an origin-enclosing surface to **V** has a topological degree of -1, then $D(\mathbf{V})$ at $\mathbf{r} = \mathbf{0}$ could have signed eigenvalues (in any order) of $++-$ or $---$. Physically, the origin could be either a saddle point or a sink for **V** with no distinction in topological degree because both $++-$ and $---$ eigenvalues multiply to a negative sign. Rather than calculating the topological degree, to try to classify the flux of energy and canonical momentum through a 3D optical field zero, we use the signs of the eigenvalues of their first-order dyadics evaluated in the position of the field zero. Due to the odd number of eigenvalues of 3D Jacobian matrices, there is a strong contrast between optical fluxes in 3D and in paraxial fields [38].

We use the ideas discussed here to report our findings in the following sub-sections, beginning with the six possible ways that C lines and L lines can intersect in a 3D zero.

C. Polarization Singularities at a 3D Electric Field Zero

We will focus on a 3D electric field zero in position $\mathbf{r}_0$, that is, $\mathbf{E}(\mathbf{r}_0) = \mathbf{0}$, and study the nearby strands of circular and linear electric polarization. Identical arguments to those given here could

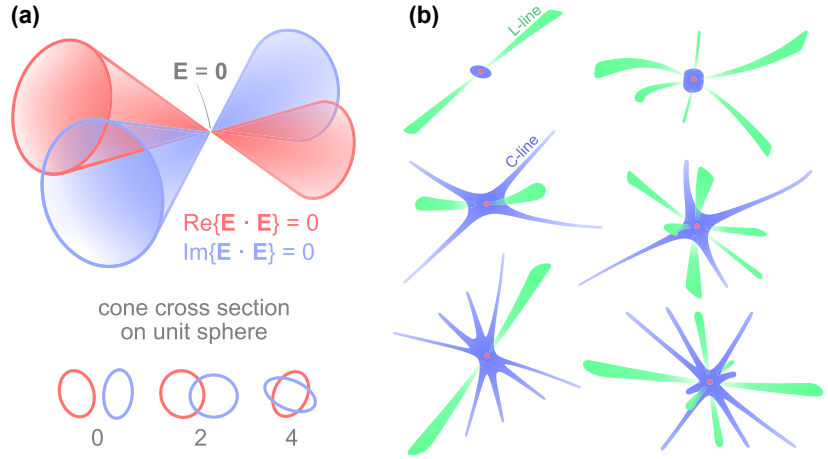

Fig. 2. Electric polarization singularities passing through a 3D electric field zero at position $\mathbf{r}_0$. (a) Visualization of why zero, two, or four C lines must pass through $\mathbf{r}_0$. In a first-order approximation, surfaces $\mathrm{Re}\{\mathbf{E}\cdot\mathbf{E}\}=0$ (red) and $\mathrm{Im}\{\mathbf{E}\cdot\mathbf{E}\}=0$ (blue) are double cones, and where they intersect, C lines exist. Two double cones intersect along two or four lines, or do not intersect at all, which is easy to see by considering the cones' cross sections on the unit sphere: ellipses that cross at zero, two, or four points. (b) Six different examples of electric field zeros created at position $\mathbf{r}_0$ (red circle), one per unique combination of C lines and L lines meeting there. The C lines are marked by blue regions where $\mathbf{E}\cdot\mathbf{E}\approx 0$ and the L lines by green regions where $\mathrm{Im}\{\mathbf{E}^*\times\mathbf{E}\}\approx\mathbf{0}$. Each field zero is created in analytical simulations in MATLAB by designing the polarization of 10 plane waves with random wave vectors, wavelength 500 nm, to interfere destructively at $\mathbf{r}_0$. The plane waves have different polarizations and wave vectors for each example zero in (b).

be made for magnetic field zeros [$\mathbf{H}(\mathbf{r}_0)=\mathbf{0}$] and magnetic polarization singularities, or for simultaneous electric and magnetic field zeros [$\mathbf{E}(\mathbf{r}_0)=\mathbf{H}(\mathbf{r}_0)=\mathbf{0}$] and polarization singularities of either $\mathbf{E}$ or $\mathbf{H}$. Any smooth function of $\mathbf{r}$ is nearly linear over small distances, which means all fundamental behavior of the electric field in the immediate vicinity of the zero is captured by its Jacobian, $\mathbf{J}_\mathrm{E}=D(\mathbf{E})$, a complex 3×3 matrix containing all first-order spatial derivatives of E_x, E_y, and E_z, evaluated at $\mathbf{r}_0$:

$$\mathbf{J}_\mathrm{E}=D(\mathbf{E})=\begin{pmatrix}\frac{\partial E_x}{\partial x} & \frac{\partial E_x}{\partial y} & \frac{\partial E_x}{\partial z}\\ \frac{\partial E_y}{\partial x} & \frac{\partial E_y}{\partial y} & \frac{\partial E_y}{\partial z}\\ \frac{\partial E_z}{\partial x} & \frac{\partial E_z}{\partial y} & \frac{\partial E_z}{\partial z}\end{pmatrix}=(\nabla\otimes\mathbf{E})^T. \tag{2}$$

The Jacobian of the magnetic field at $\mathbf{r}_0$, $\mathbf{J}_\mathrm{H}$, can be defined similarly. In free space, $\mathbf{J}_\mathrm{E}$ and $\mathbf{J}_\mathrm{H}$ are always traceless because $\mathbf{E}$ and $\mathbf{H}$ are divergence free. Maxwell's equations also require that if $\mathbf{E}(\mathbf{r}_0)=\mathbf{0}$, then $\mathbf{J}_\mathrm{H}$ must be symmetric at $\mathbf{r}_0$ and vice versa for $\mathbf{H}(\mathbf{r}_0)=\mathbf{0}$. We make a first-order approximation of the electric field vector near $\mathbf{r}_0$ with

$$\tilde{\mathbf{E}}=\mathbf{J}_\mathrm{E}\mathbf{v}, \tag{3}$$

where $\mathbf{v}=\mathbf{r}-\mathbf{r}_0$.

Nearby C lines emerge in our approximated field wherever $\tilde{\mathbf{E}}\cdot\tilde{\mathbf{E}}=0$, which we may calculate using Eq. (3) and separate into real and imaginary parts:

$$\begin{aligned}\tilde{\mathbf{E}}\cdot\tilde{\mathbf{E}}&=(\mathbf{J}_\mathrm{E}\mathbf{v})\cdot(\mathbf{J}_\mathrm{E}\mathbf{v})\\ &=\mathbf{v}^T\mathbf{M}\mathbf{v}+i\mathbf{v}^T\mathbf{N}\mathbf{v},\end{aligned} \tag{4}$$

where $\mathbf{M}=\mathrm{Re}\{\mathbf{J}_\mathrm{E}^T\mathbf{J}_\mathrm{E}\}$, and $\mathbf{N}=\mathrm{Im}\{\mathbf{J}_\mathrm{E}^T\mathbf{J}_\mathrm{E}\}$. The two terms in Eq. (4) are quadric surfaces connecting constant valued real and imaginary parts of $\tilde{\mathbf{E}}\cdot\tilde{\mathbf{E}}$, and the real and imaginary surfaces described by setting Eq. (4) equal zero cross in real space where $\tilde{\mathbf{E}}$ is circularly polarized. The real 3×3 matrices $\mathbf{M}$ and $\mathbf{N}$ are symmetric and always have real eigenvalues. Normally, these eigenvalues have signs $++-$ or $--+$ (in any order) so that surfaces $\mathbf{v}^T\mathbf{M}\mathbf{v}=0$ and $\mathbf{v}^T\mathbf{N}\mathbf{v}=0$ are both double cones, vertices touching at $\mathbf{v}=\mathbf{0}$ as shown in Fig. 2(a). The cones have an elliptical cross section whose ellipticity is constant with distance from $\mathbf{v}=0$ in the linear approximation. Because two ellipses can intersect at zero, two, or four points [as shown in the lower part of Fig. 2(a)], there must be zero, two, or four C lines passing through the electric field zero. If one matrix, say $\mathbf{M}$, is positive or negative definite (all positive or all negative eigenvalues), $\mathrm{Re}\{\tilde{\mathbf{E}}\cdot\tilde{\mathbf{E}}\}$ will solely increase or decrease in all outward directions from $\mathbf{v}=\mathbf{0}$. Then, the constant-valued surface $\mathbf{v}^T\mathbf{M}\mathbf{v}=C$ becomes an ellipsoid, and $\mathbf{v}^T\mathbf{M}\mathbf{v}=0$ is satisfied only at $\mathbf{v}=\mathbf{0}$ so that no C lines pass through the 3D vortex.

To reveal the number of L lines that extend through the 3D electric field zero, we must calculate the electric field spin, given by

$$\mathbf{S}_\mathrm{E}\propto\mathrm{Im}\{\mathbf{E}^*\times\mathbf{E}\}=2\,\mathrm{Re}\{\mathbf{E}\}\times\mathrm{Im}\{\mathbf{E}\}. \tag{5}$$

When the electric field is linearly polarized ($\mathbf{S}_\mathrm{E}=\mathbf{0}$), the real and imaginary parts of $\mathbf{E}$ must be (anti)parallel. Under the approximation Eq. (3), this means

$$\mathrm{Re}\{\mathbf{J}_\mathrm{E}\}\mathbf{v}=\lambda\,\mathrm{Im}\{\mathbf{J}_\mathrm{E}\}\mathbf{v}, \tag{6}$$

where λ is a positive or negative scalar. The directions of the L lines crossing through $\mathbf{v}=\mathbf{0}$ are given by the three eigenvectors of the matrix $\mathrm{Im}\{\mathbf{J}_\mathrm{E}\}^{-1}\mathrm{Re}\{\mathbf{J}_\mathrm{E}\}$. Since this matrix is real-valued, either all three of these eigenvectors are real, corresponding to three L lines, or only one of them is real and is accompanied by a conjugate pair of complex eigenvectors. In that case, just one L line passes through the 3D zero because $\mathbf{v}$ cannot point in a complex direction.

Summarizing, zero, two, or four C lines and either one or three L lines always meet at $\mathbf{r}_0$ in a 3D electric field zero $\mathbf{E}(\mathbf{r}_0)=\mathbf{0}$. An identical conclusion can be drawn for C lines and L lines of the magnetic field for the case of $\mathbf{H}(\mathbf{r}_0)=\mathbf{0}$. In Fig. 2(b), an example of each of the six possible C line/L line combinations through a 3D zero is presented, the zeros created in the interference of 10 plane waves. Each zero is enforced by separate ensembles of 10 plane

waves with random wave vector directions that are deliberately polarized to destructively interfere at a single point.

D. Energy Flux Singularity

The flow of energy in a light field is described by the complex Poynting vector, $\frac{1}{2}\mathbf{E}^* \times \mathbf{H}$. The real part of this vector (often itself called the "Poynting vector") corresponds to the time-averaged power transfer (sometimes known as active power) in the field, while reactive power (associated with oscillations in the transfer of power) is accounted for by the less-used imaginary part. We refer to these two real vectors as $\mathbf{P}_\mathrm{r}$ and $\mathbf{P}_\mathrm{i}$:

$$\mathbf{P}_\mathrm{r} = \frac{1}{2}\,\mathrm{Re}\{\mathbf{E}^* \times \mathbf{H}\}, \tag{7}$$

$$\mathbf{P}_\mathrm{i} = \frac{1}{2}\,\mathrm{Im}\{\mathbf{E}^* \times \mathbf{H}\}. \tag{8}$$

When either $\mathbf{E}$ or $\mathbf{H}$ is zero at point $\mathbf{r}_0$, the complex Poynting vector vanishes, and its real and imaginary parts circulate in the space around the zero according to their first-order derivatives at $\mathbf{r}_0$. The real part $\mathbf{P}_\mathrm{r}$ is divergence-less in free space where there is no absorption or energy generation, and must therefore be organized into a vector saddle point at $\mathbf{r}_0$. An example flow of active power around a 3D electric field zero created at $\mathbf{r}_0$ [$\mathbf{E}(\mathbf{r}_0) = \mathbf{0}, \mathbf{H}(\mathbf{r}_0) \neq \mathbf{0}$] is given in the top row of panels in Fig. 3, where $\mathbf{P}_\mathrm{r}$ is plotted on the xy, xz, and yz planes coinciding at $\mathbf{r}_0$. Although there is no net flow of active power in or out of the zero, $\mathbf{P}_\mathrm{r}$ streamlines can be arranged in two topologically different ways depending on whether the signs of the eigenvalues of its first-order dyadic, $\mathrm{Im}\{(\mathbf{J}_\mathrm{E}^T - \mathbf{J}_\mathrm{E})\mathbf{J}_\mathrm{E}^*\}$ (written electrically without prefactors), are $++-$ or $+--$, corresponding to two possible topological orders of -1 or $+1$. One might notice that the imaginary Poynting vector $\mathbf{P}_\mathrm{i}$, which is plotted on the same planes for the same free space electric field zero at $\mathbf{r}_0$ in the lower row of panels of Fig. 3, is not divergence free—in fact, it is physically possible for a source, sink, or saddle of $\mathbf{P}_\mathrm{i}$ to exist there, depending on whether $\mathbf{E}$ or $\mathbf{H}$ is zero. To see why, we first note that using Maxwell's equations in free space (see Supplement 1), the imaginary Poynting vector can be decomposed into a sum of two terms, one polarization independent and one polarization dependent, each containing electric and magnetic contributions:

$$\begin{aligned}\mathbf{P}_\mathrm{i} &= -\frac{c^2}{2\omega}\epsilon_0\,\mathrm{Re}\{(\mathbf{J}_\mathrm{E}^T - \mathbf{J}_\mathrm{E})\mathbf{E}^*\} \\ &= \frac{c^2}{2\omega}\mu_0\,\mathrm{Re}\{(\mathbf{J}_\mathrm{H}^T - \mathbf{J}_\mathrm{H})\mathbf{H}^*\} \\ &= \frac{c^2}{4\omega}\left[-\frac{1}{2}\epsilon_0\nabla(\mathbf{E}^*\cdot\mathbf{E}) + \frac{1}{2}\mu_0\nabla(\mathbf{H}^*\cdot\mathbf{H})\right] \\ &\quad + \frac{c^2}{4\omega}\,\mathrm{Re}\{\epsilon_0\mathbf{J}_\mathrm{E}\mathbf{E}^* - \mu_0\mathbf{J}_\mathrm{H}\mathbf{H}^*\}.\end{aligned} \tag{9}$$

The first term in Eq. (9) represents the difference in gradient of the electric and magnetic energy density of the light field, while polarization-dependent behavior of $\mathbf{P}_\mathrm{i}$ derives from the second term since $\mathbf{J}_\mathrm{E}\mathbf{E}^*$ and $\mathbf{J}_\mathrm{H}\mathbf{H}^*$ contain inter-component multiplication. In certain cases such as a uniformly polarized standing wave, the second term is zero, and the gradient of the difference in electric and magnetic energy density determines the direction of reactive power flow. Because $\mathbf{E}^* \cdot \mathbf{E} = |\mathbf{E}|^2$ is a positive real quantity, a 3D zero in $\mathbf{E}$ is a source for the vector $\nabla(\mathbf{E}^* \cdot \mathbf{E})$ (and likewise for $\mathbf{H}$). Depending on the combination of polarization-independent and polarization-dependent terms as per Eq. (9), the divergence of the imaginary Poynting vector at $\mathbf{r}_0$ may not be zero. Note that there is a difference in signs between the electric and magnetic terms in Eq. (9), meaning $\mathbf{P}_\mathrm{i}$ behaves differently for $\mathbf{E}(\mathbf{r}_0) = \mathbf{0}$, $\mathbf{H}(\mathbf{r}_0) \neq \mathbf{0}$ and $\mathbf{H}(\mathbf{r}_0) = \mathbf{0}$, $\mathbf{E}(\mathbf{r}_0) \neq \mathbf{0}$, and $\mathbf{E}(\mathbf{r}_0) = \mathbf{H}(\mathbf{r}_0) = \mathbf{0}$ 3D zeros. To understand the flow of $\mathbf{P}_\mathrm{i}$ through an optical field zero, we assume a non-dual electric field zero [$\mathbf{E}(\mathbf{r}_0) = \mathbf{0}$ and $\mathbf{H}(\mathbf{r}_0) \neq \mathbf{0}$] and make a first-order approximation of $\mathbf{P}_\mathrm{i}$, this time referring to the relevant linear transformation matrix as the first-order dyadic of the imaginary Poynting vector, $D(\mathbf{P}_\mathrm{i})$, which is defined identically to $\mathbf{J}_\mathrm{E}$ in Eq. (2) with $\mathbf{P}_\mathrm{i}$ and its components in place of $\mathbf{E}$. Our approximate imaginary Poynting vector is

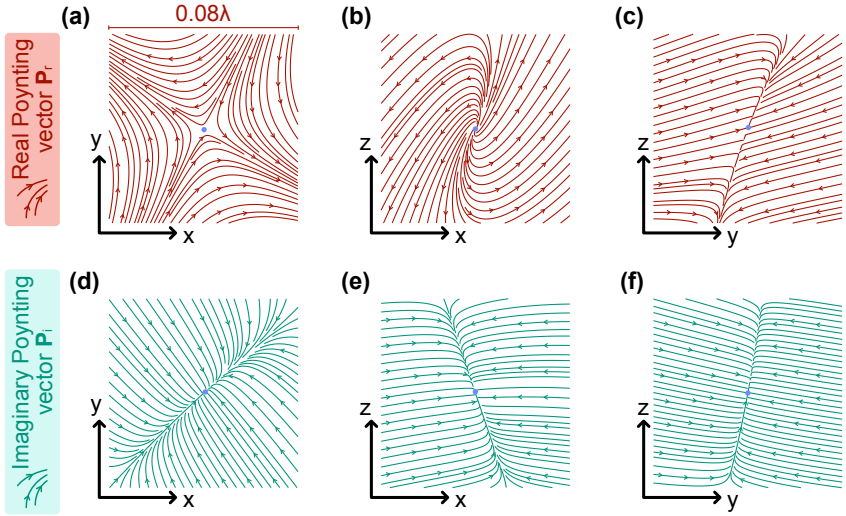

Fig. 3. Flow of the (a)–(c) real $\mathbf{P}_\mathrm{r}$ and (d)–(f) imaginary $\mathbf{P}_\mathrm{i}$ parts of the Poynting vector, $\frac{1}{2}\mathbf{E}^* \times \mathbf{H}$, on the xy, xz, and yz planes coinciding with an electric field zero at position $\mathbf{r}_0$ (blue circle). The real Poynting vector is divergence free, meaning a vector saddle point of $\mathbf{P}_\mathrm{r}$ is set up at $\mathbf{r}_0$. The imaginary Poynting vector is not necessarily divergence free and can be organized in a sink at $\mathbf{r}_0$ when $\mathbf{E}(\mathbf{r}_0) = \mathbf{0}$ (a source is not possible unless the magnetic field is zero). Results are generated by designing the polarization of 10 plane waves with random propagation directions to interfere completely at $\mathbf{r}_0$.

$$\tilde{\mathbf{P}}_i = D(\mathbf{P}_i)\mathbf{v}, \tag{10}$$

where $\mathbf{v} = \mathbf{r} - \mathbf{r}_0$. The dyadic $D(\mathbf{P}_i) = (\nabla \otimes \mathbf{P}_i)^T$ evaluated at $\mathbf{r}_0$ is, using the electric representation of $\mathbf{P}_i$ in Eq. (9) (top line),

$$D(\mathbf{P}_i) = -\frac{c^2}{2\omega}\epsilon_0 \,\mathrm{Re}\{(\mathbf{J}_E^T - \mathbf{J}_E)\mathbf{J}_E^*\}. \tag{11}$$

There are no second-order derivatives of $\mathbf{E}$ in Eq. (11) because $\mathbf{E}(\mathbf{r}_0) = \mathbf{0}$. Surprisingly, $D(\mathbf{P}_i)$ cannot have three positive eigenvalues, as justified in the Supplement 1. The result is that at a 3D electric field zero, $\mathbf{P}_i$ is organized into one of two types of saddle with topological degree 1 or -1, or a sink with topological degree -1, never a source. When $\mathbf{H}(\mathbf{r}_0) = \mathbf{0}$ and $\mathbf{E}(\mathbf{r_0}) \neq \mathbf{0}$, the opposite is true because of the dual-asymmetry of the imaginary Poynting vector: $\mathbf{P}_i$ can form a saddle or source at $\mathbf{r}_0$ but not a sink.

E. Orbital Current Singularity

When divided by c^2, the real Poynting vector Eq. (7) turns into a momentum density, kinetic momentum density, which, using Maxwell's equations for time-harmonic fields, can be split in to a well-known sum of separate orbit and spin contributions [39,40]. For instance, by substituting (with prefactors) the curl of $\mathbf{E}$ for $\mathbf{H}$, kinetic momentum density can be written as

$$\begin{aligned}\Pi &= \frac{1}{2c^2}\,\mathrm{Re}\{\mathbf{E}^* \times \mathbf{H}\} \\ &= \frac{1}{2\omega}\epsilon_0\,\mathrm{Im}\{\mathbf{E}^* \cdot (\nabla)\mathbf{E}\} + \frac{1}{2\omega}\epsilon_0 \nabla \times \frac{1}{2}\,\mathrm{Im}\{\mathbf{E}^* \times \mathbf{E}\},\end{aligned} \tag{12}$$

where $\mathbf{A}\cdot(\nabla)\mathbf{B} = A_x\nabla B_x + A_y \nabla B_y + A_z \nabla B_z = \mathbf{J}_B^T\mathbf{A}$, with $\mathbf{J}_B$ being the Jacobian of $\mathbf{B}$ defined identically to Eq. (2) (the decomposition is explained in more detail in the Supplement 1). The first decomposed term is $\mathbf{p}_E^o$, the orbital contribution to kinetic momentum density, called canonical momentum density, imparted by the electric field only:

$$\mathbf{p}_E^o = \frac{1}{2\omega}\epsilon_0\,\mathrm{Im}\{\mathbf{E}^* \cdot (\nabla)\mathbf{E}\} = \frac{1}{2\omega}\epsilon_0\,\mathrm{Im}\{\mathbf{J}_E^T\mathbf{E}^*\}. \tag{13}$$

Equation (12) can also be written purely in terms of $\mathbf{H}$, and by averaging these equivalent representations of Π, dual-symmetric canonical momentum density is obtained:

$$\mathbf{p}^o = \frac{1}{4\omega}\,\mathrm{Im}\{\epsilon_0\mathbf{E}^* \cdot (\nabla)\mathbf{E} + \mu_0\mathbf{H}^* \cdot (\nabla)\mathbf{H}\}. \tag{14}$$

This momentum density definition contains both the electric and magnetic fields' influences, and produces the total orbital angular momentum of the field within a volume when $\mathbf{r} \times \mathbf{p}^o$ is integrated. Naturally, the electric and magnetic contributions to Eq. (14) become zero whenever $\mathbf{E} = \mathbf{0}$ and $\mathbf{H} = \mathbf{0}$. Singularities in $\mathbf{E}$ ($\mathbf{H}$) are automatically coupled to singularities in the $\mathbf{p}_E^o$ ($\mathbf{p}_H^o$) vector, which has an undetermined direction in the 3D zero. This implies circulation of canonical momentum in some fashion in the surrounding volume. Of course, while the total canonical momentum density at $\mathbf{r}_0$ is not zero when only one electromagnetic field is zero, e.g., $\mathbf{E} = \mathbf{0}$, we could draw the same conclusions we make here for Eq. (14) rather than Eq. (13) near a dual-3D vortex ($\mathbf{E}(\mathbf{r}_0) = \mathbf{H}(\mathbf{r}_0) = \mathbf{0}$). Note that by normalizing $\mathbf{E}$, the argument to Im{} in Eq. (13) defines the local electric wave vector [25]:

$$\mathbf{k}_{loc}^e = -i\mathbf{e}^* \cdot (\nabla)\mathbf{e}, \tag{15}$$

where $\mathbf{e} = \frac{\mathbf{E}}{\sqrt{\mathbf{E}^*\cdot\mathbf{E}}}$. The real part of $\mathbf{k}_{loc}^e$ is the local phase gradient of the electric field, while $\mathrm{Im}\{\mathbf{k}_{loc}^e\}$ points in the direction of decreasing electric field intensity. A 3D, real vector, $\mathrm{Re}\{\mathbf{k}_{loc}^E\}$ (and therefore canonical momentum density) can vanish at localized points in space with non-zero electric field, where a saddle-like circulation of $\mathrm{Re}\{\mathbf{k}_{loc}^E\}$ surrounds [41], similar to the top row of panels in Fig. 3. But when the electric field vanishes and the direction of $\mathrm{Re}\{\mathbf{k}_{loc}^E\}$ is automatically undefined, a different behavior emerges.

To understand why, we once again make a first-order approximation, this time of $\mathbf{p}_E^o$, capturing the electric canonical momentum very near a 3D electric field zero at $\mathbf{r}_0$ in its dyadic $D(\mathbf{p}_E^o)$:

$$\tilde{\mathbf{p}}_E^o = D(\mathbf{p}_E^o)\mathbf{v}, \tag{16}$$

where $\mathbf{v} = \mathbf{r} - \mathbf{r}_0$. The dyadic $D(\mathbf{p}_E^o) = (\nabla \otimes \mathbf{p}_E^o)^T$ at a general point in space is given by

$$\begin{aligned}D(\mathbf{p}_E^o) = &\frac{1}{4\omega}\epsilon_0\,\mathrm{Im}\{\mathbf{J}_E^T\mathbf{J}_E^*\} \\ &+ \frac{1}{4\omega}\varepsilon_0\,\mathrm{Im}\{E_x^*\mathrm{Hess}(E_x) + E_y^*\mathrm{Hess}(E_y) + E_z^*\mathrm{Hess}(E_z)\},\end{aligned} \tag{17}$$

where $\mathrm{Hess}(A)$ is the Hessian matrix of the scalar field A:

$$\mathrm{Hess}(A) = \begin{pmatrix} \frac{\partial^2 A}{\partial x^2} & \frac{\partial^2 A}{\partial x \partial y} & \frac{\partial^2 A}{\partial x \partial z} \\ \frac{\partial^2 A}{\partial y \partial x} & \frac{\partial^2 A}{\partial y^2} & \frac{\partial^2 A}{\partial y \partial z} \\ \frac{\partial^2 A}{\partial z \partial x} & \frac{\partial^2 A}{\partial z \partial y} & \frac{\partial^2 A}{\partial z^2} \end{pmatrix}. \tag{18}$$

As $\mathbf{E}$ approaches zero, the trace-less matrix $D(\mathbf{p}_E^o)$ is dominated by the first term in Eq. (17), and if evaluated at a location $\mathbf{r}_0$, where $\mathbf{E}(\mathbf{r}_0) = \mathbf{0}$, the linear approximation of $\mathbf{p}_E^o$ responds only to the properties of the matrix in the first term of Eq. (17), $\mathrm{Im}\{\mathbf{J}_E^T\mathbf{J}_E^*\}$. This is an anti-symmetric matrix which always has one zero and two purely imaginary eigenvalues, meaning that in the direction of the one real eigenvector of $D(\mathbf{p}_E^o)$ at $\mathbf{r}_0$, the approximated electric canonical momentum does not increase at all, producing a zero-momentum line. The imaginary eigenvalues of $D(\mathbf{p}_E^o)$ twists $\mathbf{p}_E^o$ into a surrounding vortex-like structure. This special type of vector field singularity is called a circulation. Fundamentally, the canonical momentum should only be zero at confined points in general 3D fields, so this apparent vortex line is preserved only locally to the electric field zero at $\mathbf{r}_0$, dissolving with distance as higher-order derivatives of $\mathbf{p}_E^o$ become significant (it is, in fact, just a very elongated null point of $\mathbf{p}_E^o$). The direction of the vortex pseudo-line in the vicinity of the electric field zero is also given by the curl of the orbital current:

$$\begin{aligned}\mathbf{D} = \nabla \times \mathbf{p}_E^o \propto &\mathrm{Re}\{\nabla E_x\} \times \mathrm{Im}\{\nabla E_x\} + \mathrm{Re}\{\nabla E_y\} \\ &\times \mathrm{Im}\{\nabla E_y\} + \mathrm{Re}\{\nabla E_z\} \times \mathrm{Im}\{\nabla E_z\}.\end{aligned} \tag{19}$$

We visualize this feature in Fig. 4, where a 3D electric field zero is created at point $\mathbf{r}_0$ by deliberately polarizing 10 plane waves, each with random wave vectors, to destructively interfere at $\mathbf{r}_0$. The real part of the electric local wave vector, $\mathrm{Re}\{\mathbf{k}_{loc}^e\}$, the real part of Eq. (15), is calculated, and the region of space where $|\mathrm{Re}\{\mathbf{k}_{loc}^e\}| < 0.1k$ ($k = \frac{2\pi}{\lambda}$) is revealed by a red line approximately 0.1λ in length. The electric local wave vector is proportional to $\mathbf{p}_E^o$ and shows the direction of canonical momentum carried by

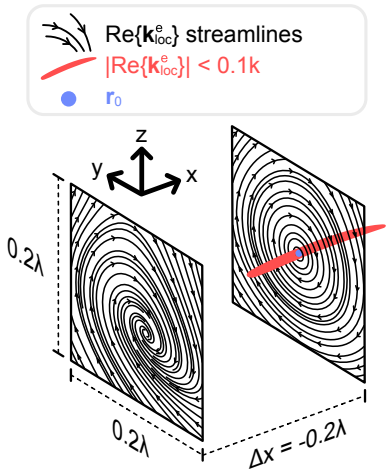

Fig. 4. Vortex pseudo-line (red) of the real electric local wave vector, $\mathrm{Re}\{\mathbf{k}^{\mathrm{e}}_{\mathrm{loc}}\}$, passing though an electric field zero at position $\mathbf{r}_0$ (blue circle), that is, $\mathbf{E}(\mathbf{r}_0)=\mathbf{0}$ and $\mathbf{H}(\mathbf{r}_0)\neq\mathbf{0}$. The red line indicates regions of space where $|\mathrm{Re}\{\mathbf{k}^{\mathrm{e}}_{\mathrm{loc}}\}|<0.1k$, where $k=\frac{2\pi}{\lambda}$. The line is roughly oriented along the x axis, and the electric local wave vector is plotted on two different yz planes, one coinciding with $\mathbf{r}_0$ and the other at an x displacement of $\Delta x=-0.2\lambda$. A cylindrical, vortex circulation of $\mathrm{Re}\{\mathbf{k}^{\mathrm{e}}_{\mathrm{loc}}\}$ appears on the plane coinciding with $\mathbf{r}_0$, but this circulation loses symmetry and definition when moving away from $\mathbf{r}_0$, signaling a discontinuous vortex "line" passing through the 3D zero. Results are generated from interference of 10 plane waves with random wave vectors deliberately polarized to create a 3D electric field zero at $\mathbf{r}_0$.

the electric field. This red line is not continuous; $\mathrm{Re}\{\mathbf{k}^{\mathrm{e}}_{\mathrm{loc}}\}$ actually vanishes only at $\mathbf{r}_0$, but it increases in magnitude so slowly in a certain direction (direction of the real eigenvector of $\mathrm{Im}\{\mathbf{J}_{\mathrm{E}}^{T}\mathbf{J}_{\mathrm{E}}^{*}\}$) that a line-like structure of $|\mathrm{Re}\{\mathbf{k}^{\mathrm{e}}_{\mathrm{loc}}\}|\approx 0$ exists very near $\mathbf{r}_0$, stirring the electric canonical momentum into a local vortex. This is shown by the two yz planes on which $\mathrm{Re}\{\mathbf{k}^{\mathrm{e}}_{\mathrm{loc}}\}$ is plotted in Fig. 4. The real part of the electric local wave vector forms a swirl around the red line, a swirl losing definition if the plotting plane is too far from $\mathbf{r}_0$. This remarkable structure always appears when all three electric field components are zero together at a point.

F. Spin Current

The second term in the decomposition of kinetic momentum density, as represented in Eq. (12), is referred to as the spin momentum. It is proportional (and should not be confused with) the curl of the spin angular momentum of the electric, magnetic, or electromagnetic field depending on the representation. Like before, we will focus on the electric representation of the decomposed kinetic momentum density, referring to the electric spin momentum with $\mathbf{p}^{\mathrm{s}}_{\mathrm{E}}$:

$$\mathbf{p}^{\mathrm{s}}_{\mathrm{E}}=\frac{1}{2\omega}\epsilon_0\nabla\times\frac{1}{2}\,\mathrm{Im}\{\mathbf{E}^{*}\times\mathbf{E}\}=-\frac{1}{2\omega}\,\epsilon_0\mathrm{Im}\{\mathbf{J}_{\mathrm{E}}\mathbf{E}^{*}\}. \tag{20}$$

The electric spin momentum is a divergence-free vector whose dyadic $D(\mathbf{p}^{\mathrm{s}}_{\mathrm{E}})$ has three non-zero eigenvalues when evaluated in the position of an electric field zero, organizing $\mathbf{p}^{\mathrm{s}}_{\mathrm{E}}$ into one of two types of 3D vector saddle points, just like the real Poynting vector in Fig. 3. Expressing, in Eq. (20), the electric spin momentum with the electric field Jacobian reveals that only a difference in sign and orientation of $\mathbf{J}_{\mathrm{E}}$ separates $\mathbf{p}^{\mathrm{s}}_{\mathrm{E}}$ from the electric canonical momentum $\mathbf{p}^{\mathrm{o}}_{\mathrm{E}}$, given by Eq. (13). This means that, in a dual electric–magnetic zero, $\mathbf{E}(\mathbf{r}_0)=\mathbf{H}(\mathbf{r}_0)=\mathbf{0}$, where $\mathbf{J}_{\mathrm{E}}$ is symmetric from Maxwell's equations, the spin and canonical momentum dyadics are equal and opposite, $D(\mathbf{p}^{\mathrm{s}}_{\mathrm{E}})=-D(\mathbf{p}^{\mathrm{o}}_{\mathrm{E}})$ (this also means that the dyadic of the real Poynting vector is zero). In a first-order approximation of both $\mathbf{p}^{\mathrm{s}}_{\mathrm{E}}$ and $\mathbf{p}^{\mathrm{o}}_{\mathrm{E}}$ near $\mathbf{r}_0$ in this case, a zero-line exists in exactly the same place for both vectors, and around it, $\mathbf{p}^{\mathrm{s}}_{\mathrm{E}}$ and $\mathbf{p}^{\mathrm{o}}_{\mathrm{E}}$ have vortex-like circulation with opposite handedness to each other.

G. Spin Angular Momentum

The dual spin angular momentum, created by the rotation of the electric and magnetic field vectors, is given by [42]

$$\mathbf{S}=\frac{1}{4\omega}\,\mathrm{Im}\{\epsilon_0\mathbf{E}^{*}\times\mathbf{E}+\mu_0\mathbf{H}^{*}\times\mathbf{H}\}. \tag{21}$$

The electric and magnetic parts individually describe the ellipticity of the electric and magnetic polarization ellipses, pointing in the direction perpendicular to the ellipse plane. Once more for simplicity, we will focus on the singularity in the electric field spin angular momentum, $\mathbf{S}_{\mathrm{E}}=\frac{1}{4\omega}\,\mathrm{Im}\{\epsilon_0\mathbf{E}^{*}\times\mathbf{E}\}$, left in a 3D electric field zero positioned at $\mathbf{r}_0$. The total spin angular momentum, Eq. (21), is not zero if only $\mathbf{E}(\mathbf{r}_0)=\mathbf{0}$, but we could draw similar conclusions for $\mathbf{S}$ as we do here for $\mathbf{S}_{\mathrm{E}}$ when the electric and magnetic fields are simultaneously zero at $\mathbf{r}_0$.

Decomposing $\mathbf{S}_{\mathrm{E}}$ using Maxwell's equations, we can write its first-order dyadic at $\mathbf{r}_0$ in terms of the light field Jacobian matrices (see Supplement 1):

$$D(\mathbf{S}_{\mathrm{E}})=\frac{1}{4\omega^2}\epsilon_0\,\mathrm{Re}\{(\mathbf{J}_{\mathrm{H}}^{T}-\mathbf{J}_{\mathrm{H}})\mathbf{J}_{\mathrm{E}}^{*}\}. \tag{22}$$

We note that Eq. (22), describing the spatial derivatives of the electric field spin only, depends on the magnetic field Jacobian matrix $\mathbf{J}_{\mathrm{H}}$, which is automatically symmetric whenever $\mathbf{E}=\mathbf{0}$ from Maxwell's equations. The consequence is that $\mathbf{J}_{\mathrm{H}}^{T}-\mathbf{J}_{\mathrm{H}}=\mathbf{0}$ and all elements of $D(\mathbf{S}_{\mathrm{E}})$ at $\mathbf{r}_0$ are zero when $\mathbf{E}(\mathbf{r}_0)=\mathbf{0}$. Higher-order derivatives of $\mathbf{S}_{\mathrm{E}}$ (Hessian matrices for each component) need to be calculated to fully understand the flux of the electric spin angular momentum in the neighborhood of a 3D zero in $\mathbf{E}$.

H. Dual Rotations of 3D Zeros

A key symmetry of the electromagnetic field is its dual symmetry, which is that the electric and magnetic field vectors (true for instantaneous fields and phasors) can be replaced with transformed vectors, $\mathbf{E}\rightarrow\mathbf{E}'$ and $\mathbf{B}\rightarrow\mathbf{B}'=\mu_0\mathbf{H}'$, according to a continuous transformation, while retaining their relationship through Maxwell's equations. We use the $\mathbf{B}$ field as the dual of $\mathbf{E}$ in this section for consistency with literature. This property has interesting implications for 3D zeros, making a clear distinction between asymmetric zeros (such as $\mathbf{E}=\mathbf{0}$, $\mathbf{B}\neq\mathbf{0}$) and symmetric, "true" zeros ($\mathbf{E}=\mathbf{B}=\mathbf{0}$). The electric and magnetic fields can be continuously transformed over an angle θ via [43,44]

$$\mathbf{E}\rightarrow\mathbf{E}'=\mathbf{E}\cos\theta+\mathbf{B}\sin\theta, \tag{23}$$

$$\mathbf{B}\rightarrow\mathbf{B}'=\mathbf{B}\cos\theta-\mathbf{E}\sin\theta. \tag{24}$$

In an asymmetric electric field zero, $\mathbf{E}=\mathbf{0}$, $\mathbf{B}\neq\mathbf{0}$, Eqs. (23) and (24) simplify to $\mathbf{E}'=\mathbf{B}\sin\theta$ and $\mathbf{B}'=\mathbf{B}\cos\theta$. It is easy to see that in this case, for θ values equal to quarters of 2π, the asymmetric zero may be completely exchanged between the transformed

Table 1. Summary of the Seven Dyadics (Numbered) that Classify the Vector Field Singularities Organized by a 3D Electric Field Zero[a]

	Dyadic at $\mathbf{r}_0$	Associated Singularity	Singularity Type	Dyadic Characteristic
	$\mathbf{J}_E$	Electric field $\mathbf{E}$	Saddle	Electric field Jacobian
1.	$\mathrm{Im}\{\mathbf{J}_E\}^{-1}\mathrm{Re}\{\mathbf{J}_E\}$	L lines	n/a	Number of real eigenvalues is number of L lines
2.	$\mathrm{Re}\{\mathbf{J}_E^T\mathbf{J}_E\}$	C lines	n/a	Dyadics 2 and 3 define quadric surfaces M and N, respectively; intersection lines of M and N are C lines
3.	$\mathrm{Im}\{\mathbf{J}_E^T\mathbf{J}_E\}$	C lines	n/a	
4.	$\mathrm{Im}\{\mathbf{J}_E^T\mathbf{J}_E^*\}$	Local wave vector $\mathbf{k}_{\mathrm{loc}}^e$	Circulation	Real eigenvector gives the axis of $\mathbf{k}_{\mathrm{loc}}^e$ vortex
5.	$-\mathrm{Im}\{\mathbf{J}_E\mathbf{J}_E^*\}$	Spin current $\mathbf{p}_E^s$	Saddle	
6.	$\mathrm{Im}\{(\mathbf{J}_E^T-\mathbf{J}_E)\mathbf{J}_E^*\}$	Real Poynting vector $\mathbf{P}_r$	Saddle	Eigenvalue signs give exact topology of minimum
7.	$-\mathrm{Re}\{(\mathbf{J}_E^T-\mathbf{J}_E)\mathbf{J}_E^*\}$	Imaginary Poynting vector $\mathbf{P}_i$	Saddle or sink	

[a]Dyadics 1–3 are constructed matrices related to the number of crossing polarization singularity lines. Dyadics 4–7 are proportional to the Jacobian matrices of the point vector singularities coupled to the 3D zero, so their eigenvalues relate directly to the flux of the vector through the singularity.

electric and magnetic fields. For every other value of θ, the transformed electric and magnetic fields are parallel and in-phase, drawing ellipses with the same ellipticity and orientation, with an amplitude ratio of $\tan\theta$. The real Poynting vector is invariant to dual rotations and remains zero throughout the transformation. Given the ranging of $\tan\theta$ between $\pm\infty$, we can make the alternative statement that any zero in the real Poynting vector can be transformed into a 3D zero in either the $\mathbf{E}$ or $\mathbf{B}$ field. Parallel components of $\mathbf{E}$ and $\mathbf{B}$, as are present for arbitrary values of θ, are responsible for magnetoelectric light–matter interactions [45]. Meanwhile, a true zero $\mathbf{E}=\mathbf{B}=\mathbf{0}$ is not affected by transformation Eqs. (23) and (24), for any value of θ, as both electric and magnetic fields stay zero.

I. Summary Table

In Table 1, we summarize the seven dyadics that classify the number of crossing C lines and L lines, the flux of the real and imaginary parts of the Poynting vector, the spin current, and the orientation of the canonical momentum vortex pseudo-line existing at a 3D electric field zero, $\mathbf{E}(\mathbf{r}_0)=\mathbf{0}$, while $\mathbf{H}(\mathbf{r}_0)\neq\mathbf{0}$. To characterize a magnetic field zero, the matrices can be written magnetically by substituting $\mathbf{J}_E$ for $\mathbf{J}_H$ (and changing the $-$ sign in front of matrix 7 to a $+$), in which case matrices 1, 2, and 3 characterize magnetic polarization singularities and matrices 4 and 5 the magnetic local wave vector and spin current, respectively. In the case of a dual-3D zero, $\mathbf{E}(\mathbf{r}_0)=\mathbf{H}(\mathbf{r}_0)=\mathbf{0}$, matrices 6 and 7 are zero because both $\mathbf{J}_E$ and $\mathbf{J}_H$ are symmetric.

3. DISCUSSION

3D optical field zeros are codimension 6 entities that, unlike axial zeros in beams, are completely localized, the optical field growing brighter in all outward directions. Although they rarely occur naturally in light (requiring three additional parameters beyond spatial x, y, z due to their codimension), 3D zeros can be deliberately created in plane wave interference or in the near fields of light-scattering matter [21] to reveal the unusual features they imprint in the light field's energy, wave vector, and polarization structures. Both with mathematical argument and by creating field zeros in plane wave interference, we showed that whenever the electric or magnetic field is zero at point $\mathbf{r}_0$, then some combination of zero, two, or four C lines, lines of pure circular polarization, and one or three L lines, lines of pure linear polarization of the field in question, intersect at $\mathbf{r}_0$. Likewise, an imprint is made at $\mathbf{r}_0$ in the surrounding flux of the parts of the complex Poynting vector $\frac{1}{2}\mathbf{E}^*\times\mathbf{H}$, local wave vector, spin momentum, and spin angular momentum, each organized in a vector source, sink, or saddle point. The signs of the eigenvalues of the first-order dyadics of each quantity at $\mathbf{r}_0$ reveal this. Of particular interest is canonical momentum. Typically, canonical momentum vanishes at confined points in space, but a 3D zero in $\mathbf{E}$ ($\mathbf{H}$) twists electric (magnetic) canonical momentum into a sub-wavelength, vortex-like structure around an axis with an easily calculated direction. We say it is a sub-wavelength object because, although it resembles the twisted vortex structures of well-known doughnut beams, it is not preserved with increasing distance from $\mathbf{r}_0$. In the combination of the way energy flows through $\mathbf{r}_0$ and the number of intersecting polarization singularities, any 3D field zero inscribes one of a discrete number of topologically unique signatures in the electromagnetic field. We identify seven dyadics whose spectra could classify all physically possible imprints of 3D optical field zeros.

It is tempting to speculate that a surface enclosing an electric or magnetic field point zero might, in addition to the quantities already identified, possess a nonzero topological Chern number due to a nontrivial geometric phase 2-form (Berry curvature) resulting from the neighboring polarization pattern. The appropriate expression for the geometric phase 2-form is the curl of the local wave vector Eq. (15):

$$\mathbf{V}=\nabla\times\mathbf{k}_{\mathrm{loc}}^e. \tag{25}$$

Near an electric field zero, $\mathbf{V}$ is anti-symmetric; integrating over a small sphere centered on the field zero gives zero. We showed that in its neighborhood, a 3D zero in $\mathbf{E}$ constructs a local wave vector vortex with an identifiable axis along which $|\mathbf{V}|$ is very large. It is interesting that even when the complete vector characteristics of light are considered, a linear momentum vortex line still persists when all three field components are zero at a confined point. This vector field vortex is an analog to a phase vortex in a complex scalar field, with a key difference being that the vector field vortex line is not continuous. Although the electromagnetic zero has some topological effects as we described in this paper, it is not so strong as to endow a surface around it with a nonzero Chern number.

We have shown that, despite being unstable to perturbation, 3D zeros of the electric and electromagnetic fields have topological properties generalizing those of scalar vortices and polarization singularities. The minimum number of parameters needed to achieve this topological control is equal to the codimension of the complex 3D zero (i.e., six). Further studies might indicate how a 3D zero's topological properties behave under perturbation. Mathematically, the properties of such a zero are characterized in 6D space; what is realizable in physical three dimensions depends on the way the 3D submanifold, corresponding to the realized physical polarizations, sits in this 3D space. Such an analysis would also indicate how a 3D zero's structure behaves under perturbation. Since the field must smoothly adapt to the presence of the nongeneric zero, the neighborhood gains the characteristic coupled polarization, energy, and momentum structures we have described. This opens a new chapter to controlling the topological structure of complex electromagnetic fields: engineering other nongeneric, special points, lines, or other structures may demonstrate geometric, topological, and physical properties beyond what is possible in the usual features engineered in structured light. By highlighting the unusual properties of 3D field zeros, we hope to inspire new applications not achievable with the commonly used, lower-dimensional dark spots, such as those in cylindrical beams or simple standing waves.

Funding. Engineering and Physical Sciences Research Council (EP/R513064/1); European Research Council (ERC2016-STG-714151-PSINFONI).

Acknowledgment. We thank Sinuhé Perea-Puente for a mathematical proof.

Author Contribution. A.J.V. conducted mathematical analyses and simulations; M.R.D. gave direction to and supervised the research; F.J.R-F. supervised the research. All authors contributed to the manuscript; A.J.V. wrote the first draft.

Disclosures. The authors declare no conflicts of interest.

Data availability. Data underlying the results presented in this paper are not publicly available at this time but may be obtained from the authors upon reasonable request.

Supplemental document. See Supplement 1 for supporting content.

REFERENCES

1. K. O'Holleran, M. R. Dennis, and M. J. Padgett, "Topology of light's darkness," Phys. Rev. Lett. **102**, 143902 (2009).
2. J. Leach, M. R. Dennis, J. Courtial, and M. J. Padgett, "Knotted threads of darkness," Nature **432**, 165 (2004).
3. K. O'Holleran, M. J. Padgett, and M. R. Dennis, "Topology of optical vortex lines formed by the interference of three, four, and five plane waves," Opt. Express **14**, 3039–3044 (2006).
4. M. R. Dennis, R. P. King, B. Jack, K. O'Holleran, and M. J. Padgett, "Isolated optical vortex knots," Nat. Phys. **6**, 118–121 (2010).
5. S. J. Tempone-Wiltshire, S. P. Johnstone, and K. Helmerson, "Optical vortex knots-one photon at a time," Sci. Rep. **6**, 24463 (2016).
6. D. Kleckner and W. T. M. Irvine, "Creation and dynamics of knotted vortices," Nat. Phys. **9**, 253–258 (2013).
7. C. N. Weiler, T. W. Neely, D. R. Scherer, A. S. Bradley, M. J. Davis, and B. P. Anderson, "Spontaneous vortices in the formation of Bose-Einstein condensates," Nature **455**, 948–951 (2008).
8. M. B. Hindmarsh and T. W. B. Kibble, "Cosmic strings," Rep. Prog. Phys. **58**, 477 (1995).
9. X. Guo, J. Zhong, P. Li, B. Wei, S. Liu, and J. Zhao, "Creation of topological vortices using Pancharatnam-Berry phase liquid crystal holographic plates," Chin. Phys. B **29**, 040305 (2020).
10. L. Wang, W. Zhang, H. Yin, and X. Zhang, "Ultrasmall optical vortex knots generated by spin-selective metasurface holograms," Adv. Opt. Mater. **7**, 1900263 (2019).
11. P. Li, X. Guo, J. Zhong, S. Liu, Y. Zhang, B. Wei, and J. Zhao, "Optical vortex knots and links via holographic metasurfaces," Adv. Phys. X **6**, 1843535 (2021).
12. W. Zhang, K. Wei, L. Huang, D. Mao, B. Jiang, F. Gao, G. Zhang, T. Mei, and J. Zhao, "Optical vortex generation with wavelength tunability based on an acoustically-induced fiber grating," Opt. Express **24**, 19278–19285 (2016).
13. S. W. D. Lim, J.-S. Park, M. L. Meretska, A. H. Dorrah, and F. Capasso, "Engineering phase and polarization singularity sheets," Nat. Commun. **12**, 4190 (2021).
14. F. Balzarotti, Y. Eilers, K. C. Gwosch, A. H. Gynnå, V. Westphal, F. D. Stefani, J. Elf, and S. W. Hell, "Nanometer resolution imaging and tracking of fluorescent molecules with minimal photon fluxes," Science **355**, 606–612 (2017).
15. S. W. Hell and J. Wichmann, "Breaking the diffraction resolution limit by stimulated emission: stimulated-emission-depletion fluorescence microscopy," Opt. Lett. **19**, 780–782 (1994).
16. H. He, N. R. Heckenberg, and H. Rubinsztein-Dunlop, "Optical particle trapping with higher-order doughnut beams produced using high efficiency computer generated holograms," J. Mod. Opt. **42**, 217–223 (1995).
17. H. He, M. E. J. Friese, N. R. Heckenberg, and H. Rubinsztein-Dunlop, "Direct observation of transfer of angular momentum to absorptive particles from a laser beam with a phase singularity," Phys. Rev. Lett. **75**, 826 (1995).
18. J. Wang, J.-Y. Yang, I. M. Fazal, N. Ahmed, Y. Yan, H. Huang, Y. Ren, Y. Yue, S. Dolinar, M. Tur, and A. E. Willner, "Terabit free-space data transmission employing orbital angular momentum multiplexing," Nat. Photonics **6**, 488–496 (2012).
19. H. Huang, G. Xie, Y. Yan, N. Ahmed, Y. Ren, Y. Yue, D. Rogawski, M. J. Willner, B. I. Erkmen, K. M. Birnbaum, S. J. Dolinar, M. P. J. Lavery, M. J. Padgett, M. Tur, and A. E. Willner, "100 tbit/s free-space data link enabled by three-dimensional multiplexing of orbital angular momentum, polarization, and wavelength," Opt. Lett. **39**, 197–200 (2014).
20. A. E. Willner, K. Pang, H. Song, K. Zou, and H. Zhou, "Orbital angular momentum of light for communications," Appl. Phys. Rev. **8**, 041312 (2021).
21. A. J. Vernon and F. J. Rodríguez-Fortuño, "Creating and moving nanoantenna cold spots anywhere," Light Sci. Appl. **11**, 258 (2022).
22. C. M. Spaegele, M. Tamagnone, S. W. D. Lim, M. Ossiander, M. L. Meretska, and F. Capasso, "Topologically protected optical polarization singularities in four-dimensional space," Sci. Adv. **9**, sciadv.adh0369 (2023).
23. S. W. D. Lim, J.-S. Park, C. M. Spägele, D. Kazakov, A. H. Dorrah, M. L. Meretska, and F. Capasso, "Point singularity array with metasurfaces," Nat. Commun. **14**, 3237 (2023).
24. J. F. Nye and J. V. Hajnal, "The wave structure of monochromatic electromagnetic radiation," Proc. R. Soc. London A Math. Phys. Sci. **409**, 21–36 (1987).
25. J. F. Nye, "Lines of circular polarization in electromagnetic wave fields," Proc. R. Soc. London A Math. Phys. Sci. **389**, 279–290 (1983).
26. M. Berry and M. Dennis, "Polarization singularities in isotropic random vector waves," Proc. R. Soc. London A Math. Phys. Sci. **457**, 141–155 (2001).
27. K. Y. Bliokh, M. A. Alonso, D. Sugic, M. Perrin, F. Nori, and E. Brasselet, "Polarization singularities and Möbius strips in sound and water-surface waves," Phys. Fluids **33**, 077122 (2021).
28. K. Y. Bliokh and F. Nori, "Spin and orbital angular momenta of acoustic beams," Phys. Rev. B **99**, 174310 (2019).
29. K. Y. Bliokh, H. Punzmann, H. Xia, F. Nori, and M. Shats, "Field theory spin and momentum in water waves," Sci. Adv. **8**, eabm1295 (2022).
30. D. Sugic, R. Droop, E. Otte, D. Ehrmanntraut, F. Nori, J. Ruostekoski, C. Denz, and M. R. Dennis, "Particle-like topologies in light," Nat. Commun. **12**, 6785 (2021).
31. H. Larocque, D. Sugic, D. Mortimer, A. J. Taylor, R. Fickler, R. W. Boyd, M. R. Dennis, and E. Karimi, "Reconstructing the topology of optical polarization knots," Nat. Phys. **14**, 1079–1082 (2018).
32. M. Dennis, "Polarization singularities in paraxial vector fields: morphology and statistics," Opt. Commun. **213**, 201–221 (2002).
33. I. Freund, "Multitwist optical Möbius strips," Opt. Lett. **35**, 148–150 (2010).
34. M. R. Dennis, "Fermionic out-of-plane structure of polarization singularities," Opt. Lett. **36**, 3765–3767 (2011).

35. T. Bauer, P. Banzer, E. Karimi, S. Orlov, A. Rubano, L. Marrucci, E. Santamato, R. W. Boyd, and G. Leuchs, "Observation of optical polarization Möbius strips," Science **347**, 964–966 (2015).
36. E. Pisanty, G. J. Machado, V. Vicuña-Hernández, A. Picón, A. Celi, J. P. Torres, and M. Lewenstein, "Knotting fractional-order knots with the polarization state of light," Nat. Photonics **13**, 569–574 (2019).
37. M. V. Berry, "Index formulae for singular lines of polarization," J. Opt. A **6**, 675–678 (2004).
38. A. Bekshaev, K. Y. Bliokh, and M. Soskin, "Internal flows and energy circulation in light beams," J. Opt. **13**, 053001 (2011).
39. M. V. Berry, "Optical currents," J. Opt. A **11**, 094001 (2009).
40. K. Y. Bliokh, A. Y. Bekshaev, and F. Nori, "Optical momentum and angular momentum in complex media: from the Abraham-Minkowski debate to unusual properties of surface plasmon-polaritons," New J. Phys. **19**, 123014 (2017).
41. M. V. Berry and P. Shukla, "Geometry of 3D monochromatic light: local wavevectors, phases, curl forces, and superoscillations," J. Opt. **21**, 064002 (2019).
42. A. Y. Bekshaev, K. Y. Bliokh, and F. Nori, "Transverse spin and momentum in two-wave interference," Phys. Rev. X **5**, 011039 (2015).
43. K. Y. Bliokh, A. Y. Bekshaev, and F. Nori, "Dual electromagnetism: helicity, spin, momentum and angular momentum," New J. Phys. **15**, 033026 (2013).
44. S. M. Barnett, "Rotation of electromagnetic fields and the nature of optical angular momentum," J. Mod. Opt. **57**, 1339–1343 (2010).
45. K. Y. Bliokh, Y. S. Kivshar, and F. Nori, "Magnetoelectric effects in local light-matter interactions," Phys. Rev. Lett. **113**, 033601 (2014).